THE ASTROPHYSICAL JOURNAL, 527:719–732, 1999 December 20

RAPID X-RAY VARIABILITY OF THE BL LACERTAE OBJECT PKS 2155−304

Y. H. ZHANG,[1] A. CELOTTI,[1] A. TREVES,[2] L. CHIAPPETTI,[3] G. GHISELLINI,[4] L. MARASCHI,[5] E. PIAN,[6] G. TAGLIAFERRI,[4] F. TAVECCHIO,[5] AND C. M. URRY[7]

Received 1999 March 31; accepted 1999 August 2

ABSTRACT

We present a detailed power-density spectrum and cross-correlation analysis of the X-ray light curves of the BL Lac object PKS 2155−304, observed with *BeppoSAX* in 1997 (SAX97) and 1996 (SAX96), aimed at exploring the rapid variability properties and the interband cross-correlations in the X-rays. We also perform the same analysis on the (archival) X-ray light curve obtained with *ASCA* in 1994 (ASCA94). No large amplitude-variability event on a timescale of less than ∼1 hr is found, and light curves in different energy bands are highly correlated with a tendency for the amplitude of variability to increase with energy. The amplitude of variability is larger and the (fastest) timescale shorter as the source becomes brighter. Furthermore, while the average power-density spectra of all the light curves present pronounced, featureless, *red noise* spectra, with the power decreasing toward high temporal frequencies, the power-law slopes are somewhat different, indicating different variability properties among the three observations. We perform a cross-correlation analysis using Monte Carlo simulations to estimate the uncertainties on time lags between different bands. A significant soft lag of ∼4 hr between the 0.1–1.5 and 3.5–10 keV bands is seen in SAX96. During SAX97, in which the source showed a high X-ray state correlated with a highly active phase in gamma rays, a short soft lag (∼0.4 hr) is detected between the same energy bands. In contrast, ASCA94 presents an intermediate soft lag of about 0.8 hr. These findings indicate that the interband soft time lags are variable and suggest that the lag is longer when the source is fainter. The time dependence of variability in PKS 2155−304 is briefly discussed within a homogeneous synchrotron scenario for blazars.

Subject headings: BL Lacertae objects: individual (PKS 2155−304) — galaxies: active — X-rays: galaxies

1. INTRODUCTION

BL Lacertae objects represent a subclass of active galactic nuclei (AGNs) emitting nonthermal radiation from radio to gamma rays, even up to TeV energies. A defining property of BL Lac objects is that the radiation is strongly variable from radio to gamma rays on different timescales. The mechanisms responsible for the nonthermal emission over such a wide energy range are commonly believed to be synchrotron and inverse Compton scattering from plasma in a relativistic jet oriented at a small angle with respect to the line of sight.

PKS 2155−304 is the brightest BL Lac object at UV wavelengths and one of the brightest in the X-ray band. It was detected in gamma rays by the EGRET experiment on the *Compton Gamma Ray Observatory* (*CGRO*) (Vestrand, Stacy, & Sreekumar 1995; Sreekumar & Vestrand 1997), and it is one of the few BL Lac objects observed at TeV energies (Chadwick et al. 1999). Its broadband spectrum shows two peaks: the first one is synchrotron emission peaking at UV and/or soft X-rays as most X-ray–selected BL Lac objects (high-frequency peak BL Lac objects, HBLs; Padovani & Giommi 1995). The other one is around the gamma-ray region, and it is attributed to Compton scattering by the same high-energy electrons that are radiating via synchrotron. It has a very hard gamma-ray spectrum in the 0.1–10 GeV region, with a power-law spectral index of $\alpha_\gamma \sim 0.71$ (Vestrand et al. 1995) and a time-averaged integral flux of 4.2×10^{-11} ergs cm^{-2} s^{-1} above 300 GeV (Chadwick et al. 1999).

PKS 2155−304 has been one of the best targets of multiwavelength campaigns because of its brightness. This kind of study has proved to be a powerful tool to constrain radiation models through the study of correlated variability among different bands. The first multiwavelength campaign was performed, from radio to X-ray wavelengths, in 1991 November, by *ROSAT*, the *International Ultraviolet Explorer* (*IUE*), and ground-based telescopes, and correlated variability was observed between UV and soft X-rays with the UV lagging by ∼2 hr (Edelson et al. 1995). However, the source showed a definitely different variability behavior in the 1994 May campaign based on *IUE*, the *Extreme Ultraviolet Explorer* (*EUVE*), and *ASCA* data. Correlated variability was observed with larger amplitude at shorter wavelengths, and significant soft lags, i.e., the UV lagging the EUV by 1 day and the EUV, in turn, lagging the X-rays by 1 day (Urry et al. 1997).

Variability can be characterized by the power-density spectrum (PDS) and interband correlations: the PDS slopes and the measured time lags impose strong constraints on radiation models. The three long-duration and high time-resolution observations by *BeppoSAX* and *ASCA* are rather suitable for carrying out temporal studies. In the present paper, we perform detailed timing analysis for these

[1] International School for Advanced Studies, SISSA/ISAS, via Beirut 2-4, I-34014 Trieste, Italy; yhzhang@sissa.it, celotti@sissa.it.
[2] Dipartimento di Scienze, Università dell'Insubria, Polo di Como, via Lucini 3, I-22100 Como, Italy; treves@uni.mi.astro.it.
[3] Istituto di Fisica Cosmica G. Occhialini, IFCTR/CNR, via Bassini 15, I-20133 Milano, Italy; lucio@ifctr.mi.cnr.it.
[4] Osservatorio Astronomico di Brera, via Bianchi 46, I-22055 Merate, Italy; ghisellini@merate.mi.astro.it, tagliaferri@merate.mi.astro.it.
[5] Osservatorio Astronomico di Brera, via Brera 28, I-20121 Milano, Italy; maraschi@brera.mi.astro.it, fabrizio@brera.mi.astro.it.
[6] Istituto TESRE/CNR, via Gobetti 101, I-40129 Bologna, Italy; pian@tesre.bo.cnr.it.
[7] Space Telescope Science Institute, 3700 San Martin Drive, Baltimore, MD 21218; cmu@stsci.edu.

observations and compare the results. Preliminary cross-correlation analysis with Monte Carlo simulations were first reported in Treves et al. (1999).

We briefly summarize the observations in § 2. The light curves and variability analysis are presented in § 3, followed by the PDS analysis in § 4. In § 5, we carry out a comprehensive cross-correlation analysis with detailed Monte Carlo simulations to determine the uncertainties on interband lags. The physical implications of the results are discussed in § 6, and conclusions are drawn in § 7.

2. OBSERVATIONS

The *BeppoSAX* payload (Boella et al. 1997a) consists of four Narrow Field Instruments (NFIs) that point in the same direction, namely, one Low Energy Concentrator Spectrometer (LECS), sensitive in the 0.1–10 keV range (Parmar et al. 1997), and three identical Medium Energy Concentrator Spectrometers (MECS) sensitive in 1.5–10 keV band (Boella et al. 1997b). Both the LECS and MECS detectors are Gas Scintillation Proportional Counters (GSPC) and are in the focus of the four identical X-ray telescopes. There are two more collimated instruments: the High Pressure Gas Scintillation Proportional Counter (HPGSPC) (Manzo et al. 1997) and the Phoswich Detector System (Frontera et al. 1997), but these, however, are not suitable for performing temporal analysis because of the high background and limited statistics on a source like PKS 2155−304. Therefore, for the following timing analysis, only LECS and MECS data are used.

BeppoSAX NFIs observed PKS 2155−304 for more than 2 days during the Performance Verification phase on 1996 November 20–22 (SAX96) and for slightly less than 1.5 days during our AO1 observation on 1997 November 22–24 (SAX97). The effective exposure times for MECS and LECS were 63 ks and 22 ks for SAX97, and 108 ks and 36 ks for SAX96, respectively. The *BeppoSAX* data reduction procedure is described in detail by Chiappetti et al. (1999). The light curves were first presented by Giommi et al. (1998) and Chiappetti et al. (1999). In particular, in the latter work the presence of a soft lag of about 10^3 s and a tendency of the amplitude of variability to increase with energy have been found in the SAX97 data.

PKS 2155−304 was also monitored by the *ASCA* satellite for more than 2 days on 1994 May 19–21 (ASCA94), which was coordinated with a multiwavelength monitoring from radio to X-rays (Pesce et al. 1997; Pian et al. 1997; Urry et al. 1997). *ASCA* includes two SIS and two GIS focal-plane detectors (Tanaka, Inoue, & Holt 1994). The X-ray light curve considered here—retrieved from the archive—was taken from the GIS detectors. Preliminary results were presented by Makino et al. (1996).

In this paper we will perform a detailed temporal analysis of the different observations and compare the relative results. The log of the three observations is shown in Table 1.

3. VARIABILITY ANALYSIS

We analyze the light curves with the timing analysis software package XRONOS.[8] Unless otherwise specified, we separate a priori the energy ranges into the following three bands: (1) 0.1–1.5 keV as the soft energy band referred to as the LE band; (2) 1.5–3.5 keV as the first medium X-ray band, which we refer to as the ME1 band; (3) 3.5–10 keV as the second medium-energy band, namely, the ME2 band. Note that the LE band of the *ASCA* observation is 0.5–1.5 keV.

The light curves binned over 1000 or 2000 s are shown in Figures 1, 2, and 3 for the SAX97, SAX96, and ASCA94 observations, respectively. We compute the hardness ratios (HR) of ME1 to LE (HR1) and of ME2 to ME1 (HR2), which are also presented in the same figures.

3.1. *Variability Parameters*

To quantify the variability properties here, we summarize the general definition of the fractional rms variability parameter $F_{\rm var}$ (e.g., Rodríguez-Pascual et al. 1997). The data series $F_i(t)$ of the light curve has a standard deviation $\sigma_F^2 = (1/N-1)\sum_{i=1}^{N}[F_i(t)-\overline{F}]^2$, where $\overline{F}$ is the mean count rate. In addition, we define the *expected variance*, due to random errors $\sigma_i(t)$ associated with $F_i(t)$, as $\Delta_F^2 = (1/N)\sum_{i=1}^{N}\sigma_i^2(t)$. The *excess variance*, $\sigma_{\rm exc}$, is then defined as the difference between the standard deviation σ_F^2 and the expected variance Δ_F^2, i.e., $\sigma_{\rm exc}^2 = \sigma_F^2 - \Delta_F^2$, from which we can define the fractional rms variability parameter as $F_{\rm var} = \sigma_{\rm exc}/\overline{F}$.

The above parameters characterize only the mean variability of a source. However, a direct measurement of the fastest timescale on which the intensity can change is crucial as it may constrain the source size, and thus luminosity density, accretion efficiency or beaming parameters, and black hole mass. This requires identifying rapid variability events rather than the average variability properties. One often considers the so-called doubling time as a reasonable measure of the fastest and most meaningful timescale of

[8] Stella, L., & Angelini, L. 1993, XRONOS, A Timing Analysis Software Package, User's Guide, version 3.01; http://rosat.gsfc.nasa.gov/docs/xanadu/xronos/xronos.html for version 4.02.

TABLE 1

OBSERVATION LOG

Satellite	Instrument	Observing Time (UT)	Exposure (ks)	Observing Efficiency (%)
BeppoSAX.....	LECS	1997 Nov 22 16:03–Nov 24 01:35	22	22
BeppoSAX.....	MECS	1997 Nov 22 16:03–Nov 24 01:35	63	53
BeppoSAX.....	LECS	1996 Nov 20 00:16–Nov 22 13:30	36	20
BeppoSAX.....	MECS	1996 Nov 20 00:16–Nov 22 13:30	108	52
ASCA[a]	GIS	1994 May 19 04:30–May 21 07:55	100	55

[a] Only GIS data are analyzed.

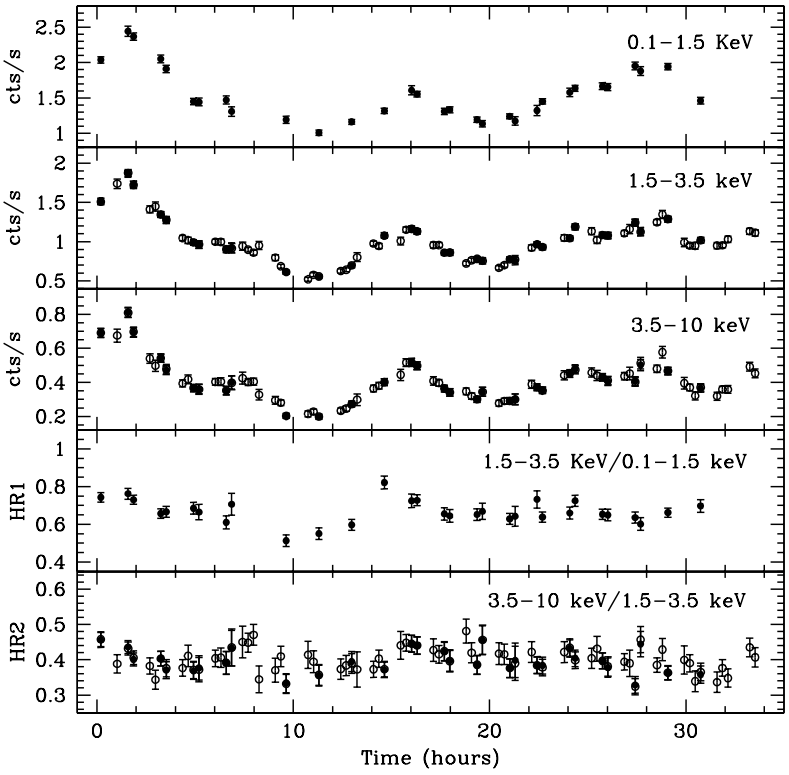

FIG. 1.—Light curves and hardness ratios of *BeppoSAX* 1997 November 22–24 observation. Data are rebinned in 1000 s. *Top to bottom*: light curve in the 0.1–1.5, 1.5–3.5, and 3.5–10 keV bands, respectively, and hardness ratio between the 1.5–3.5 and 0.1–1.5 keV bands (HR1) and between 3.5–10 and 1.5–3.5 keV bands (HR2). Note that the temporal coverage of the LECS is much more sparse than that of the MECS. Simultaneous data points between LECS and MECS are indicated by filled symbols. HR1 shows a clear correlation with the source brightness, which is not present for HR2.

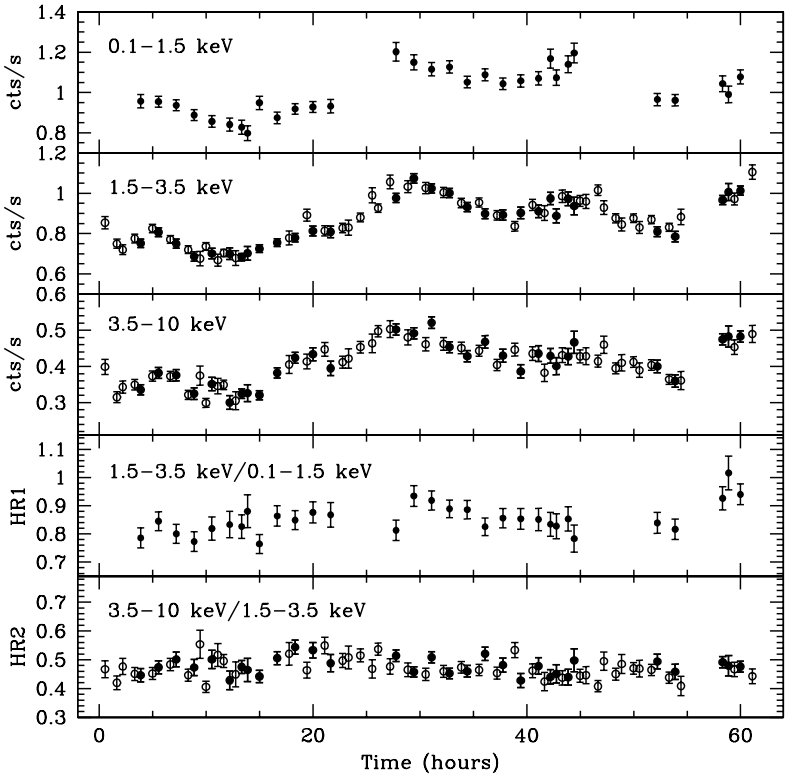

FIG. 2.—Light curves and hardness ratios of *BeppoSAX* 1996 November 20–22 observation. Data are rebinned in 2000 s. Symbols have the same meaning as in Fig. 1. HR1 (but not HR2) correlates well with the source intensity.

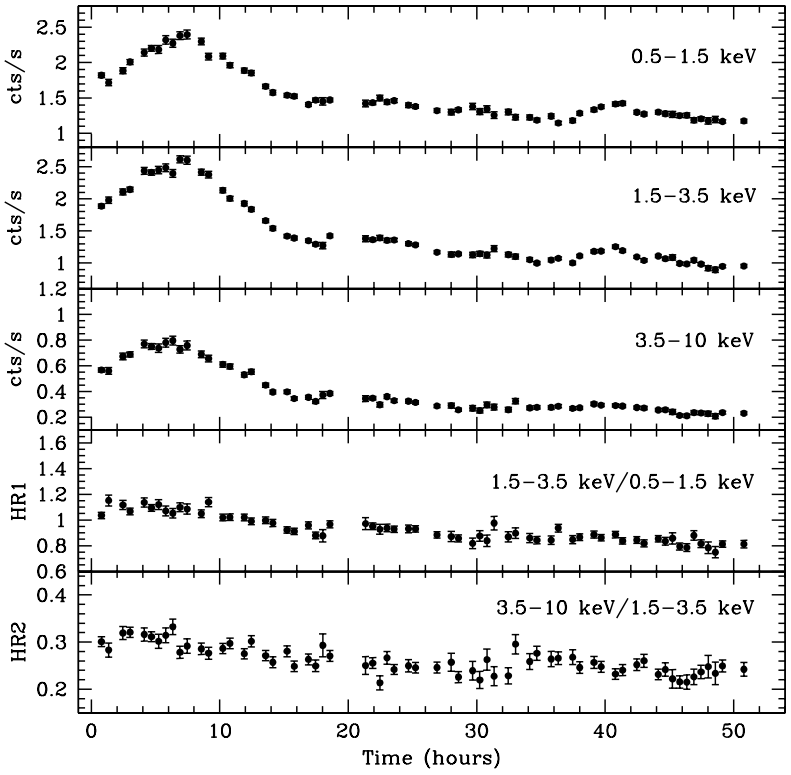

FIG. 3.—Light curves and hardness ratios of *ASCA* 1994 May 19–21 observation. Data are rebinned in 2000 s. Symbols have the same meaning as in Fig. 1. Both HR1 and HR2 closely follow the source intensity trend.

a source (e.g., Edelson 1992). More precisely, here we define the "doubling time" as $T_2 = |F\,\Delta T/\Delta F|$, where $\Delta T = T_j - T_i$, $\Delta F = F_j - F_i$, and $F = (F_j + F_i)/2$, and consider the minimum value of T_2^{ij} over any data pairs as the shortest timescale for each observation, keeping in mind that this quantity is ill-defined and depends strongly on sampling rate, length, and the signal-to-noise ratio of the observation (Press 1978). The error on T_2^{ij} is propagated through the errors on the fluxes F_i and F_j, and, a priori, we neglect the value of T_2^{ij} if the error is larger than 20%.

The variability parameters defined above are reported in Table 2.

TABLE 2

VARIABILITY PARAMETERS[a]

Band (keV)	Flux[b]	$\overline{F}$ (cts s^{-1})	σ_F (cts s^{-1})	Δ_F (cts s^{-1})	$\sigma_{\rm exc}$ (cts s^{-1})	$F_{\rm var}$	χ^2(dof)[c]	T_2 (hr)
				SAX97				
0.1–1.5.....	16.6	1.56	0.36	0.08	0.35	0.22	1711(86)	3.37 ± 0.61
1.5–3.5.....	6.78	1.00	0.28	0.06	0.27	0.27	4270(215)	1.94 ± 0.29
3.5–10	4.02	0.40	0.13	0.04	0.12	0.30	2171(215)	1.81 ± 0.31
1.5–10	10.8	1.41	0.40	0.08	0.39	0.28	6192(215)	2.04 ± 0.28
				SAX96				
0.1–1.5.....	11.9	1.01	0.12	0.07	0.10	0.10	462(141)	22.11 ± 4.16
1.5–3.5.....	4.46	0.87	0.12	0.06	0.11	0.13	1811(383)	14.46 ± 2.59
3.5–10	2.88	0.41	0.07	0.04	0.06	0.13	1156(383)	8.17 ± 1.61
1.5–10	7.34	1.28	0.18	0.07	0.16	0.13	2509(383)	9.96 ± 1.88
				ASCA94				
0.5–1.5.....	11.9	1.51	0.34	0.08	0.33	0.22	5933(330)	5.61 ± 1.08
1.5–3.5.....	5.40	1.42	0.47	0.08	0.46	0.33	11981(330)	4.83 ± 0.93
3.5–10	3.76	0.38	0.17	0.04	0.16	0.43	5824(330)	4.53 ± 0.89
1.5–10	9.16	1.81	0.63	0.09	0.62	0.35	17191(330)	4.89 ± 0.67

[a] All parameters in this table refer to a 300 s binning. See the text for the definition of each parameter.
[b] Mean flux in unit of 10^{-11} ergs cm^{-2} s^{-1}.
[c] Constant fits.

3.2. *Results*

3.2.1. *SAX97*

Figure 1 presents the light curves and hardness ratios. At the beginning of the observation, PKS 2155−304 exhibited a large flare, with a variation by a factor ~ 4, followed by two other events of smaller amplitude. The second flare presents similar rising and declining timescales. As shown in Table 2, the variability amplitude is, to some extent, different in the three bands, increasing with increasing energy ($F_{\rm var}$ is 0.22, 0.27, and 0.30 in the LE, ME1, and ME2 bands, respectively). No variations on timescales of less than ~ 1 hr are found. The most rapid variation event—the fastest among the three observations—occurred during the first flare, with minimum values of T_2 of about 3.4, 1.9, and 1.8 hr in the LE, ME1, and ME2 bands, respectively. We notice that these timescales are much shorter and the fluxes about 50% higher than those of SAX96 (see Table 2), indicating faster variability with higher intensity.

From the two panels at the bottom of Figure 1, one can see that the HR1 presents a global trend similar to that of the intensities (see Chiappetti et al. 1999 for more details). However, no statistically significant correlation seems to be present, as HR1 has the same value during the first two peaks, which have significantly different intensities, and is smaller during the end of the observation, although the average intensity is similar to that of the second peak. HR2 does not show any trend.

3.2.2. *SAX96*

As is shown in Figure 2, an approximately symmetric flare was seen in the middle of the observation, which is well resolved with similar rising and decaying timescales. A flare of lower intensity is visible at the beginning, while a larger flare probably occurred toward the end of the observation, although the observation is incomplete. Some small-amplitude variability is also detected.

The $F_{\rm var}$ values are comparable for the ME1 and ME2 bands (~ 0.13) and are $\sim 30\%$ larger than that relative to the LE band. The estimated "doubling times" are about 22, 14, and 8 hr for the LE, ME1, and ME2 bands, respectively. From Figures 1 and 2 and Table 2, it is clear that during SAX96, PKS 2155−304 was in a relatively faint state with smaller amplitude and longer timescale variability as compared with that of the SAX97 observation.

The hardness ratio HR1 shows a behavior similar to that of the light curves, in the sense that the spectrum is harder at higher intensities, while again HR2 does not follow any trend (see Fig. 2).

3.2.3. *ASCA94*

The light curves and hardness ratios relative to this observation are plotted in Figure 3. A large-amplitude flare, with an approximately symmetric shape, is seen clearly at the beginning of the observation, although the rising portion of the event is not fully sampled. PKS 2155−304 was more variable in this period than during the other two observations, as can be seen from $F_{\rm var}$ (Table 2), with a flux intermediate between SAX97 and SAX96. The estimated "doubling times" are about 5.6, 4.8, and 4.5 hr in the LE, ME1, and ME2 bands, respectively.

A significant characteristic of ASCA94 is that the hardness ratios present a trend of linear decrease over the whole period, which is a general signature that the spectra become softer when the source is fainter. Urry et al. (1997) showed the same trend through the spectral fits.

4. PDS ANALYSIS

The variability of an AGN can be statistically characterized by its PDS. The PDSs of a very few Seyfert galaxies and of PKS 2155−304 generally behave as power laws, proportional to $f^{-\alpha}$ over some temporal frequency range, where f is the temporal frequency (e.g., Edelson & Nandra 1999; Hayashida et al. 1998; Tagliaferri et al. 1991). For PKS 2155−304, the durations of the observations considered here are much longer (~ 2 days) than previous ones (e.g., *EXOSAT*), which allowed us to determine the PDS over a range extending toward relatively lower frequencies. Because of the low-exposure efficiency of the LECS ($\sim 20\%$), here we focus on the *BeppoSAX* MECS and *ASCA* light curves in the 1.5–10 keV region.

The PDS analysis is carried out with the direct Fourier transform algorithm included in the timing series analysis package XRONOS. For these observations, the PDS is calculated for the background-subtracted light curves with 10 s time resolution, as each PDS in our cases approaches (white) noise level before $\sim 10^{-2}$ Hz, which is clearly smaller than the Nyquist frequency of 5×10^{-2} Hz at 10s bin size. The average count rate is subtracted from the bins before the PDS is calculated. To improve the signal-to-noise ratio and study the mean variability properties of PKS 2155−304, the light curves are divided into several short intervals with each interval sampling 4096 points. The SAX97 light curve presents three good intervals; the SAX96 light curve has four good intervals, although we neglect the last part of the light curve, which contains a long interruption toward the end of the observation; the ASCA94 observation is divided into four good intervals. For each light curve, the power spectra from each interval are then averaged.

An important issue, discussed in detail by Tagliaferri et al. (1991), is the data gap filling, which is unavoidable for a low-orbit X-ray satellite. The gap-filling procedure could strongly affect the derived PDS slope by artificially increasing the power at high frequencies and introducing spurious quasi-periodic oscillations (QPOs) (Tagliaferri et al. 1996). To decrease the effect of data gaps in determining the PDS, we adopt the gap-filling procedure defined as "running mean gap filling" in XRONOS. This method replaces the data gaps with the moving average of the light curve, calculated in our cases over a duration of about 1.5 hr. In this way, the gaps are bridged in a smooth way, which not only simulates real events but also reduces the bias introduced by the window function. We also determined a posteriori, by considering a somewhat different duration (e.g., 2 hr), that the slope of the PDS is rather insensitive to the filling duration over which the running mean is calculated. This indicates that the running mean could follow the light curve behavior on timescales of hours, as long as the gap-filling duration is substantially shorter than the whole interval and longer than the data gaps, so that the gap center could be "linked" with the running mean from a relatively high number of points and the statistical fluctuations would be reduced.

The average PDS (after average noise subtraction) obtained in this way from each individual observation are shown in Figures 4*a*, 4*b*, and 4*c* for SAX97, SAX96, and ASCA94 light curves, respectively. These are rebinned in

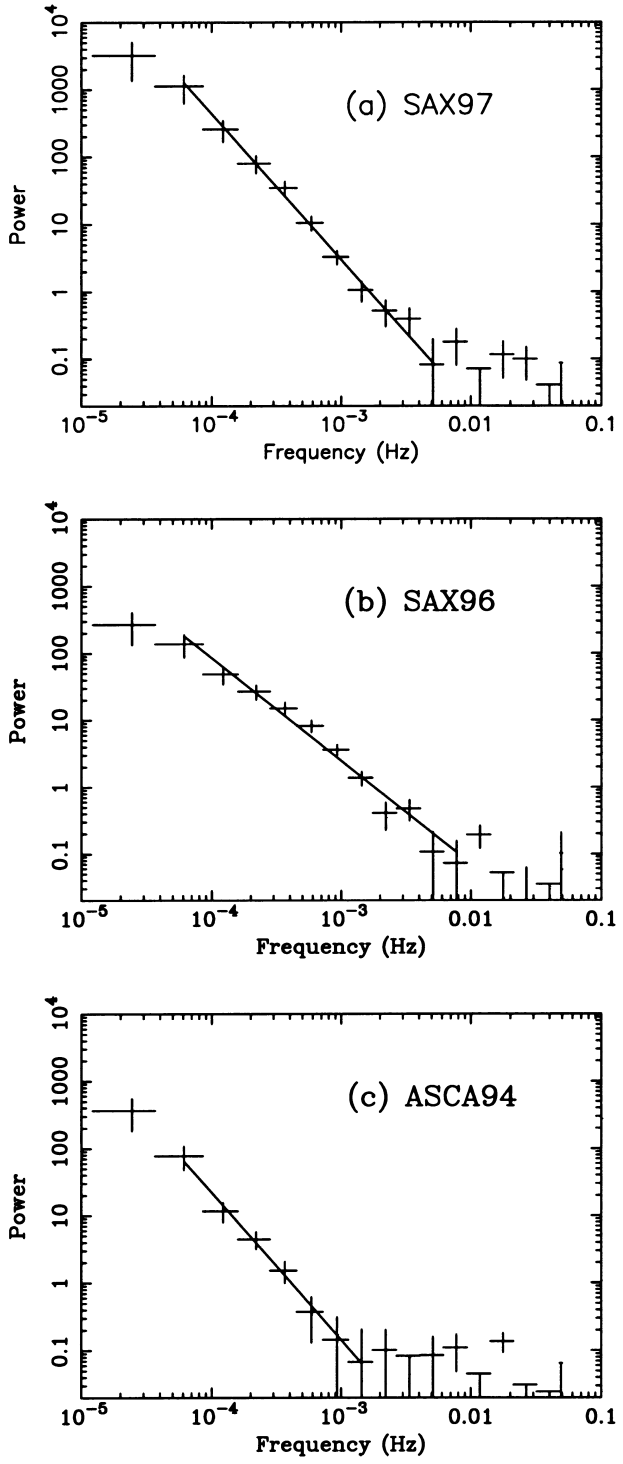

FIG. 4.—PDS with the best power-law fit (after average noise subtraction) in the 1.5–10 keV band. (*a*) SAX97; (*b*) SAX96; (*c*) ASCA94.

logarithmic intervals of 0.18 (factor 1.5) to reduce the noise and allow the estimation of error bars. This means that the first point is still the lowest frequency point, but the second point is derived by averaging the next two points, etc. In this way, the PDS values appear nearly equispaced in a log-log diagram. Each PDS is normalized so that its integral gives the squared rms fractional variability $F_{\rm var}$ (therefore the power spectrum is in units of $F_{\rm var}^2$/Hz), which is normalized to the squared average count rate. The

TABLE 3

PDS PARAMETERS

Observation	Fitting Slope[a]	χ^2(dof)[a]
SAX97.....	2.17 ± 0.10, 1.99 ± 0.10	3.4(8), 9.0(8)
SAX96.....	1.54 ± 0.07, 1.40 ± 0.07	12(9), 13(9)
ASCA94.....	2.19 ± 0.23, 2.15 ± 0.49	1.1(5), 0.9(3)

[a] The fitting region is from $\sim 6 \times 10^{-5}$ to $\sim 6 \times 10^{-3}$ Hz (SAX97), $\sim 8 \times 10^{-3}$ Hz (SAX96), and $\sim 1.5 \times 10^{-3}$ Hz (ASCA94); the second set of values in this column refers to the PDS after the removal of a linear trend.

expected (white) noise power level must be subtracted to obtain the $F_{\rm var}$ of the light curve (this level is about 1.5, 1.6, and 1.2 for SAX97, SAX96, and ASCA94 data, respectively). The error bars represent the standard deviation of the average power in each rebinned frequency interval, where the power in each bin is χ^2 distributed with $2N$ degrees of freedom and where $N = ML$ is the total number of points used to produce the mean power in each frequency bin (from M intervals and L independent Fourier frequencies).

From Figure 4, one can see that each PDS shows a strong *red noise* spectral component that decreases with increasing frequencies, without any significant narrow feature that would be indicative of periodic or quasi-periodic variability. This component approaches the noise level at $\sim 6 \times 10^{-3}$ Hz for the SAX97 and SAX96 light curves and at $\sim 1 \times 10^{-3}$ Hz for the ASCA94 data set. In addition, we note some differences among the three PDS values. The SAX97 PDS clearly shows more power than the SAX96 one at lower frequencies, indicating a flatter PDS for SAX96 (this is easy to reconcile with the fact that $F_{\rm var}$ of SAX96 [~ 0.13] is much less than that of SAX97 [$F_{\rm var} \sim 0.3$]). The ASCA94 PDS has much less power than that of SAX97 over the whole range of temporal frequencies considered here, which is consistent with the fact that the ASCA94 PDS approaches the noise level at relatively lower frequencies. However, this does not agree with their corresponding $F_{\rm var}$ values. Let us consider the origin of this discrepancy. The SAX97 and SAX96 light curves show more or less identical amplitude of variability over the whole range of observations, i.e., similar $F_{\rm var}$ for each interval, while the ASCA94 light curve does not present pronounced variability after the large flare at the beginning of the observation. Thus $F_{\rm var}$ for the ASCA94 data set significantly changes from one interval to another, being about 0.23 and 0.11 for the flare and (almost) constant flux intervals of the ASCA94 light curve, respectively, but 0.35 when calculated over the duration. This makes the ASCA94 data set more variable if we consider it as a whole. For this reason, we first computed the PDS in different intervals, normalized it so that the integral gives its own squared $F_{\rm var}$ value, and then obtained the average PDS by averaging the power spectra from each interval. Because the light curve of ASCA94 is characterized by different $F_{\rm var}$, we should use a mean value averaged from the (four) intervals considered in deriving the average PDS. This average $F_{\rm var}$, which is much smaller than those of the SAX97 and SAX96 light curves, indeed agrees well with the average PDS. Note that, instead, for the SAX97 and SAX96 light curves, the average $F_{\rm var}$ from each interval is identical to that of the whole observation.

To quantify the slope of the PDS, a power-law model is fitted to each average power spectrum in the frequency

interval $\sim 6 \times 10^{-5}$ to $\sim 6 \times 10^{-3}$ (SAX97, SAX96) or to $\sim 1.5 \times 10^{-3}$ Hz (ASCA94). The lowest frequency point of each PDS was ignored because they tend to be more noisy and also for comparison with previous PDS analysis. The best-fit power-law slopes are ~ 2.2, 1.5, and 2.2 for SAX97, SAX96, and ASCA94 PDS values, respectively. In the same way, we also compute the average PDS after the removal of a linear trend from the light curves, in which the power-law slopes for the "de-trended" PDS are consistent with the above values within 1 σ, respectively. The fitting details are shown in Table 3.

5. CROSS-CORRELATION ANALYSIS

The first clear result visible from the light curves is that the variations in the different X-ray bands are all correlated. Indeed, these intensive monitorings with high time resolution and long duration allow detailed measurements of the interband cross-correlation properties. In particular, they allow us to make quantitative estimates of the degree of correlation and of any lags between variations at different X-ray wavelengths. Two cross-correlation methods, namely the Discrete Correlation Function (DCF) and Modified Mean Deviation (MMD), are applied. In the following, a positive lag indicates the higher energy X-rays leading the lower energy ones, while a negative lag indicates the opposite.

5.1. *Cross-Correlation Analysis Technique*

5.1.1. *DCF*

The DCF is analogous to the classic correlation function (e.g., Press et al. 1992) except that it can work with unevenly sampled data. The DCF technique was described in detail by Edelson & Krolik (1988) and applied to PKS 2155−304 by Edelson et al. (1995) and Urry et al. (1997) to measure the time lags between UV and X-ray during the two multiwavelength campaigns mentioned above. Here we bin the original light curves and fix the DCF resolution according to the following criteria: (1) the bin sizes in both the light curves and the DCF should be at least 3 times smaller than any possible lag; (2) the bin size should also be as large as possible to reduce the error on the DCF. The resulting DCFs (only for the LE/ME2 case) are shown in Figures 5*a*, 5*c*, and 5*e* (*left-hand panels*) for the three observations, respectively. To quantify any time lag, we fit the DCF with a Gaussian function plus a constant and take the Gaussian centroid, rather than the DCF peak, as the lag between the two energy bands (see arguments by Edelson et al. 1995 and Peterson et al. 1998). There are two main advantages to this. First, the Gaussian fit takes into account the overall symmetry of the cross-correlation distribution around the peak, thereby reducing the possibility of spurious lags caused by a particular DCF point that could originate from statistical errors. Second, we found that, under the two conditions mentioned above, the lag and its uncertainty derived from a Gaussian fit are insensitive to the bin sizes of both the light curves and the DCF. The Gaussian fits to the DCFs are also shown in the same figures, and Table 4 reports the fitting results for the LE/ME1, ME1/ME2, and LE/ME2 cases. It should be noted that a Gaussian fit—although representative of the peak position and dispersion for both the DCF and MMD—does not necessarily provide a statistically adequate fit to these functions.

5.1.2. *MMD*

To check the results suggested by the DCF technique, we performed a similar analysis by using the MMD method introduced by Hufnagel & Bregman (1992). The MMD considers the mean deviation of the two cross-correlated time series as the correlation estimator and the minimum value of the MMD should correspond to the best correlation point (lag). Thus, unlike the DCF, it cannot be used to estimate the significance of the correlation between different wavelengths. As with the DCF, we take the centroid of a Gaussian fit as the measured lag. The MMD results with their Gaussian fits (only for the LE/ME2 case) are shown in Figures 5*b*, 5*d*, and 5*f* (*right-hand panels*), and the results of the fits are reported in Table 4 for the LE/ME1, ME1/ME2, and LE/ME2 cases.

5.2. *Monte Carlo Simulations*

As suggested by Peterson et al. (1998), the uncertainty on the cross-correlation lag is dependent on both the flux uncertainties in individual measurements and the obser-

TABLE 4

CROSS-CORRELATIONS AND LAGS: DCF AND MMD RESULTS

First Series (keV)	Second Series (keV)	DCF (hr)		MMD (hr)		r_0
		Lag	90% C.L.	Lag	90% C.L.	
SAX97						
0.1–1.5	1.5–3.5	0.30 ± 0.07	0.19, 0.41	0.17 ± 0.05	0.08, 0.26	0.92
1.5–3.5	3.5–10	0.00 ± 0.03	−0.05, 0.05	0.06 ± 0.03	0.01, 0.12	0.91
0.1–1.5	3.5–10	0.46 ± 0.07	0.34, 0.58	0.30 ± 0.06	0.20, 0.41	0.87
SAX96						
0.1–1.5	1.5–3.5	1.96 ± 0.15	1.71, 2.21	1.01 ± 0.22	0.63, 1.41	0.73
1.5–3.5	3.5–10	1.91 ± 0.10	1.74, 2.08	1.72 ± 0.18	1.40, 2.05	0.63
0.1–1.5	3.5–10	4.09 ± 0.16	3.83, 4.35	4.08 ± 0.36	3.48, 4.69	0.52
ASCA94						
0.5–1.5	1.5–3.5	0.29 ± 0.27	−0.16, 0.77	0.30 ± 0.06	0.21, 0.39	0.96
1.5–3.5	3.5–10	0.57 ± 0.30	0.09, 1.08	0.50 ± 0.06	0.39, 0.60	0.95
0.5–1.5	3.5–10	0.88 ± 0.30	0.40, 1.38	0.85 ± 0.07	0.73, 0.97	0.93

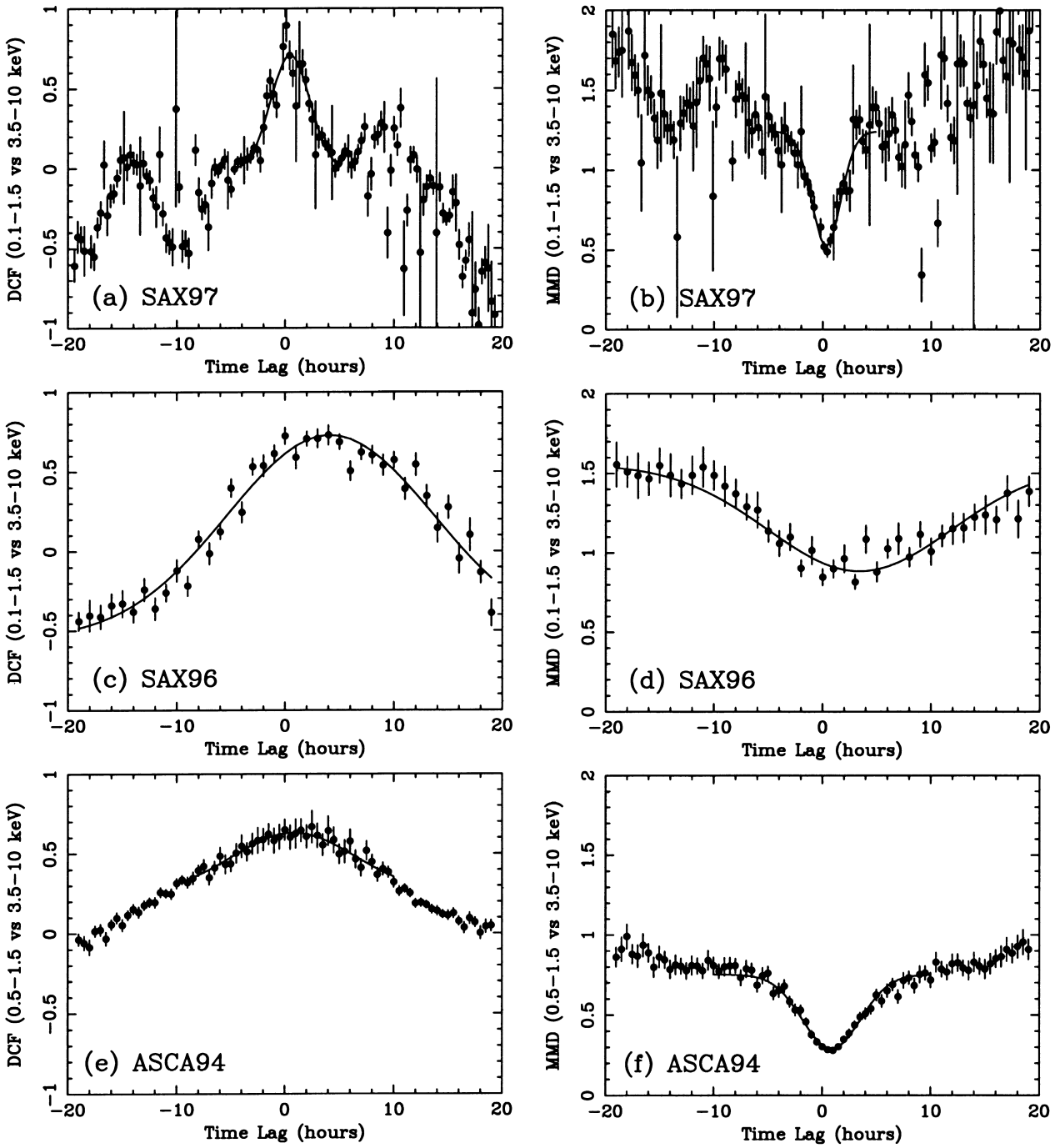

FIG. 5.—DCF and MMD between 0.1–1.5 and 3.5–10 keV. (*a*, *b*) SAX97; (*c*, *d*) SAX96; (*e*, *f*) ASCA94. Best fit consists of a Gaussian function plus a constant.

vational sampling uncertainties of the light curves. So, the statistical significance of the detection of a lag cannot be assessed just by a cross-correlation analysis. To test the dependence of our findings on photon statistics, in this section we apply to our data the model-independent Monte Carlo simulation method introduced by Peterson et al. (1998). Because of the uncertainties just mentioned, the method considers flux randomization (FR) and random subset selection (RSS). FR assumes that the errors on fluxes resulting from the total photon number in a bin (several hundred photons in our cases) are normally distributed. Thus, FR just takes each real flux F_i and modifies it by adding a random Gaussian deviation based on the quoted error σ_i for each data point of the light curves. So, the modification of each data point is statistically independent of each of the others; therefore the dependence of lags on flux errors can be assessed easily through the FR simulations. RSS tests instead the sensitivity of a cross-correlation lag by considering only subsets of the original light curves with no dependence on previous selection but still preserving the temporal order of the data points. The probability of random removal of any data point is $\sim 1/e \simeq 0.37$, which is a Poisson probability. Thus each RSS realization is based on a randomly selected subset that is typically $\sim 37\%$

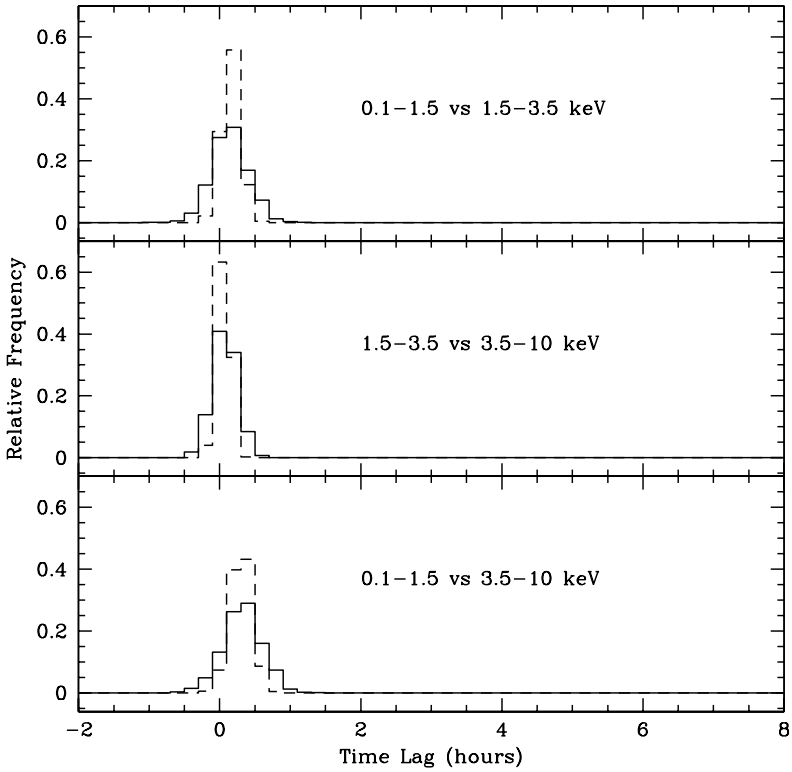

FIG. 6.—CCPD from the FR/RSS Monte Carlo simulations for the SAX97 observation. Solid and dashed lines refer to DCF and MMD results, respectively.

smaller than the real data set. Peterson et al. (1998) argue that RSS gives a fairly conservative estimate of the uncertainties caused by sampling. We thus take the combination of FR and RSS in a single simulation to test both the sensitivity of the cross-correlation lags on flux uncertainties and the sampling characteristics. We apply the DCF and the MMD to each FR/RSS Monte Carlo realization to determine individual lags obtained from the centroid of the Gaussian fit to each independent realization. The same process is repeated 2000 times to build up a cross-correlation peak distribution (CCPD; Maoz & Netzer 1989), which is not necessarily a normal distribution (e.g., Peterson et al. 1998). The CCPDs for the three observations are displayed in Figures 6, 7, and 8 (their different widths result from the different photon statistics), respectively. From the CCPD we can determine the probability that a given lag falls in some particular likelihood range. In our cases (2000 realizations), we determine the lower (upper) extrema of the 68% and 90% confidence ranges by taking the 320th (1680th) and 100th (1900th) smallest values from

TABLE 5

RESULTS OF THE FR/RSS SIMULATIONS

FIRST SERIES (keV)	SECOND SERIES (keV)	DCF (hr)			MMD (hr)		
		Lag	68% C.L.	90% C.L.	Lag	68% C.L.	90% C.L.
				SAX97			
0.1–1.5	1.5–3.5	0.14	−0.10, 0.40	−0.28, 0.57	0.16	0.04, 0.28	−0.05, 0.36
1.5–3.5	3.5–10	0.07	−0.10, 0.25	−0.22, 0.35	0.06	−0.03, 0.15	−0.09, 0.20
0.1–1.5	3.5–10	0.32	0.06, 0.59	−0.15, 0.78	0.31	0.16, 0.45	0.05, 0.55
				SAX96			
0.1–1.5	1.5–3.5	1.95	1.00, 2.92	0.28, 3.64	1.18	0.39, 1.96	−0.01, 2.84
1.5–3.5	3.5–10	2.14	1.38, 2.89	0.87, 3.43	1.77	1.04, 2.48	0.68, 3.10
0.1–1.5	3.5–10	4.27	3.21, 5.30	2.52, 6.04	4.30	3.03, 5.60	2.10, 6.59
				ASCA94			
0.5–1.5	1.5–3.5	0.32	−0.40, 1.04	−0.87, 1.53	0.31	0.12, 0.51	−0.02, 0.63
1.5–3.5	3.5–10	0.44	−0.27, 1.18	−0.84, 1.70	0.52	0.24, 0.80	0.14, 0.99
0.5–1.5	3.5–10	0.85	0.15, 1.59	−0.25, 2.10	0.88	0.58, 1.18	0.39, 1.40

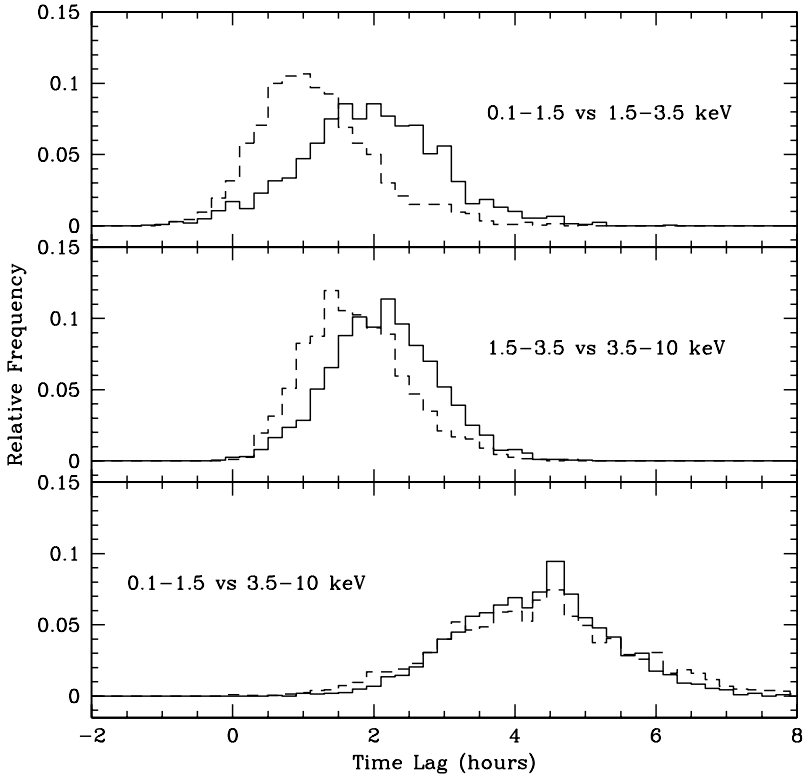

FIG. 7.—CCPD from the FR/RSS Monte Carlo simulations for the SAX96 observation

all realizations, respectively. The results of the simulations are shown in Table 5. In addition, we tested that the results are insensitive to the bin sizes of both the light curves and the cross-correlation.

In Figure 9, the lags derived from the DCF/MMD methods directly and through the simulations are compared: indeed they are fully consistent within the uncertainties estimated from the FR/RSS simulations.

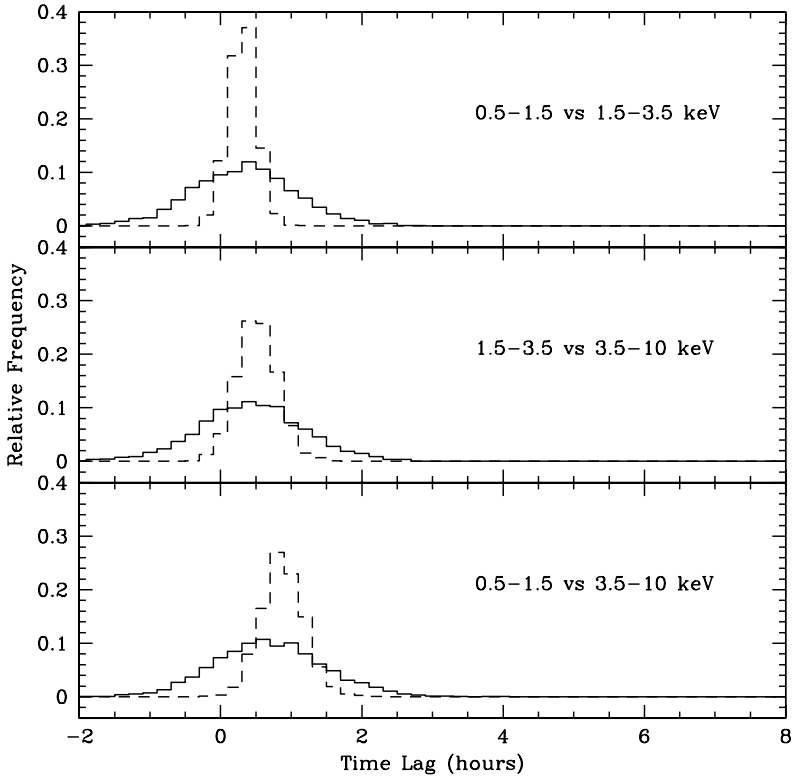

FIG. 8.—CCPD from the FR/RSS Monte Carlo simulations for the ASCA94 observation

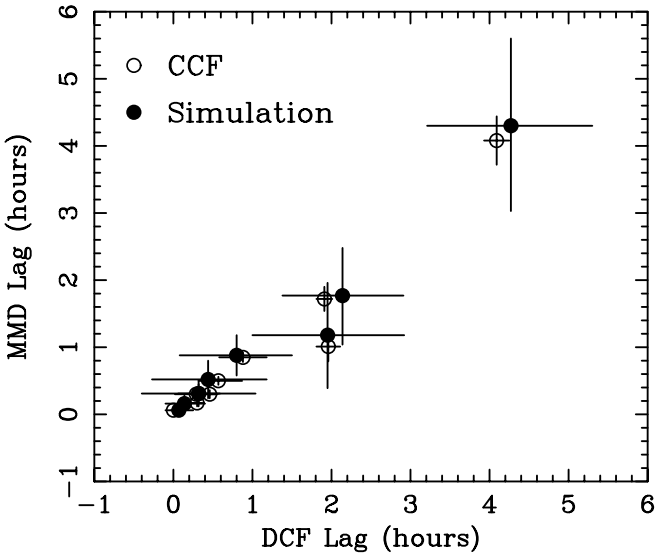

FIG. 9.—Comparison of the lags derived directly from the DCF/MMD methods with those estimated from the FR/RSS Monte Carlo simulations.

5.3. *Results*

5.3.1. *SAX97*

We remind the reader that during SAX97 the source was in a relatively high state compared with SAX96, and variability was more pronounced. The interband correlation coefficients r_0 (see Table 4) indicate that the X-rays in different bands are highly correlated. The cross-correlation analysis shows a very short soft lag between the LE and ME2 bands ($\sim$1000 s), while the lags for LE/ME1 and ME1/ME2 are consistent with zero (see Figs. 5*a*, 5*b*, and Table 4). The FR/RSS Monte Carlo simulations confirm these findings with high significance (see Fig. 6 and Table 5).

5.3.2. *SAX96*

The values of r_0 derived for LE/ME1, ME1/ME2, and LE/ME2 correlations (see Table 4) suggest that the light curves are also strongly correlated during this relatively faint state. However, in contrast to SAX97, we find significant soft X-ray lags relative to higher energy X-rays. It is apparent from Figures 5*c*, 5*d*, and 7 and Tables 4 and 5 that the lags estimated with the DCF and MMD methods are compatible within the uncertainties of the FR/RSS Monte Carlo simulations, thus indicating the presence of a soft positive lag of $\sim$4 hr between the LE and ME2 bands. Soft lags of about 2 hr are also shown by the LE/ME1 and ME1/ME2 cross-correlation functions. Note also that the soft X-ray lags in this case are the largest recorded so far for BL Lac objects in the X-rays.

5.3.3. *ASCA94*

The state of the source during the ASCA94 observation is intermediate among the two *BeppoSAX* observations. Also, these data show strong correlations among the different bands (see Table 4). The DCF and MMD analysis (see Figs. 5*e*, 5*f*, and Table 4) reveal soft lags intermediate between those of the SAX97 and SAX96 data sets: the LE lags the ME2 by about 0.8 hr, while LE lags ME1 and ME1 lags ME2 by $\sim$0.4 hr. These results are also confirmed by the FR/RSS Monte Carlo simulations (see Fig. 8 and Table 5).

5.3.4. *Comparisons*

The results from the three observations corresponding to different intensity states of PKS 2155−304 suggest that the soft time lags are variable and possibly related to the source intensity, with the soft lag becoming larger when the source is fainter. We illustrate this behavior in Figure 10*a*, where the lags between LE and ME2 are plotted against the mean fluxes in the ME2 band. A similar behavior is also present

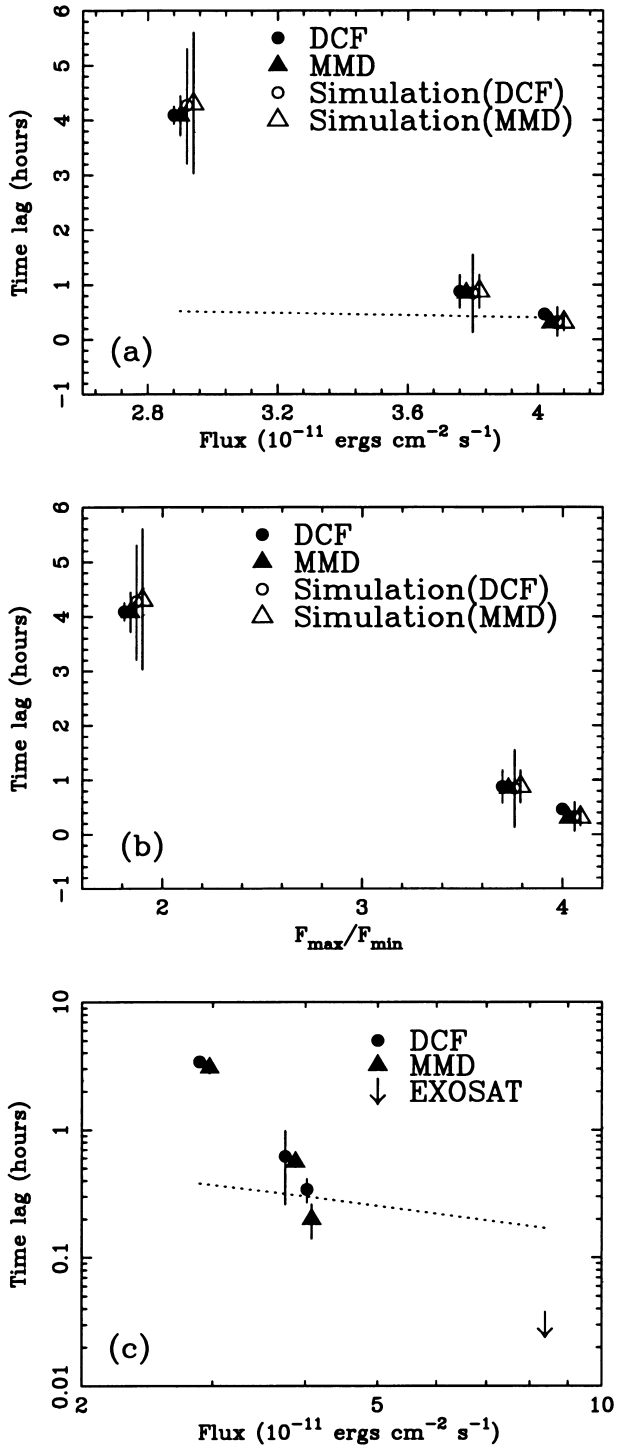

FIG. 10.—(*a*) Time lags (0.1–1.5 keV vs. 3.5–10 keV) are plotted against the fluxes in the 3.5–10 keV band. (*b*) Time lags, same as in (*a*), vs. ratios of the maximum to the minimum fluxes in the 3.5–10 keV band. (*c*) (Logarithm of) the lags (0.1–2 keV vs. 3–6 keV) with respect to the fluxes in the 3.5–10 keV band (the upper limit to the lag for the *EXOSAT* 1985 October 24 light curve is taken from Tagliaferri et al. 1991). The dotted line refers to the relation predicted by the homogeneous synchrotron model. In order to show individual errors on the lags, a small shift is applied to the flux values.

between the lags and the ratios of the maximum to the minimum count rate (see Fig. 10*b*). As a comparison, in Figure 10*c* we include the upper limit to the soft lag between the 0.1–2 and the 3–6 keV bands obtained from the *EXOSAT* observation of 1985 October 24 (Tagliaferri et al. 1991). This figure shows a power-law relation (logarithmic axis) between the lags and the fluxes. This suggestive trend might give crucial clues on the emission processes and physical parameters in PKS 2155−304 and strongly requires the comparison with the results of time-dependent emission models.

We also notice that the lags (τ) are qualitatively anticorrelated with the correlation coefficients (r_0) between the different energy bands. From Table 4, it can be seen that the r_0 values of SAX97 and ASCA94 are significantly higher than those of SAX96. On the contrary, the soft lags of SAX97 and ASCA94 are smaller than those of SAX96. This anticorrelation is indeed expected. If obvious soft lags were present, the maximum amplitude of the cross-correlation function would be significantly shifted away from the zero lag point and, thus, the standard correlation coefficient r_0 would obviously decrease if the cross-correlation function were a smooth Gaussian function (but not necessarily). Therefore, variable lags in different states are qualitatively suggested by the variable correlation degrees without any measured time shift. This behavior occurs also between the τ and r_0 within the different interband correlations (for example, the lags become larger with r_0 becoming smaller in SAX96).

Interestingly, variations of the soft lags found here in the X-ray bands are reminiscent of the variations of the UV lags with respect to the X-ray (from ~ 2 hr to ~ 2 days) between the 1991 and 1994 intensity states of this same source (see § 1).

6. DISCUSSION

The high degree of correlation and time lags between variations at different wavelengths provide strong constraints on the physical parameters of blazars. The previous multiwavelength monitoring campaigns of PKS 2155−304 found different variability behaviors (Edelson et al. 1995; Urry et al. 1997). In particular, the 1991 campaign showed the soft X-ray leading the UV by just ~ 2 hr (the result of the cross-correlation analysis was recently confirmed by Peterson et al. 1998 on the basis of simulations similar to those used in this paper). However, during the 1994 campaign, the UV lagged the X-ray by ~ 2 days. Time lags of the soft compared with the hard X-rays were suggested by the *ASCA* observations of PKS 2155−304 and Mrk 421 (Makino et al. 1996; Takahashi et al. 1996), while *EXOSAT* observations of PKS 2155−304 showed no evidence of lags, with upper limits of a few hundred seconds (Tagliaferri et al. 1991).

To interpret the interband variable time lags, the development of time-dependent models that take into account the effects of particle injection/acceleration, cooling, and diffusion would be required. However, the time-dependent problem is, in general, very complicated and only some simplified and specific cases have been considered so far. Mastichiadis & Kirk (1997) showed that, within the assumptions of an homogeneous SSC model, an increase in the maximum energy of the injected electron population can reproduce the rapid X-ray flares as well as the spectral evolution of blazars like Mrk 421. Interestingly, they also show that these features cannot be caused by changes of both the magnetic field and the amount of injected electrons. In addition, Chiaberge & Ghisellini (1999) pointed out the importance, for both spectral evolution and time lags, of delays caused by light crossing the radiating region. This effect is superposed to the wavelength dependent timescales caused by the different cooling times of radiating electrons. In contrast to the above studies, Georganopoulos & Marscher (1998) modeled, using a time-dependent inhomogeneous accelerating jet model, the evolution of flares during the two multiwavelength campaigns on PKS 2155−304. Within this scenario, the different variability features could be reproduced by assuming that plasma disturbances with different physical properties occur in an underlying jet characterized by the same physical parameters. The small time lag between the UV and X-ray bands in the 1991 November campaign would indicate quasi-cospatiality of the regions radiating at these frequencies, assuming an injected electron distribution similar to that characterizing the underlying jet emission. However, the clear time lag between these same bands in the 1994 May campaign is interpreted as an indication of spatial separation of the emitting regions. The separation can be caused by the propagation downstream of the electrons while progressively radiating at lower frequencies. This, however, also requires the injected electrons to be narrower in energy than during the 1991 November event.

Clearly, to pin down the origin and nature of variations, both systematic observational trends and a thorough analysis with the different models are needed. In this work, we have concentrated on the first aspect, but let us examine the simplest (and analytical) considerations one can draw from the observational results.

Obviously, the homogeneous synchrotron self-Compton model is the simplest interpretation for the X-ray emission and overall spectral energy distribution (SED) of PKS 2155−304 (e.g., Chiappetti et al. 1999). According to this picture, a quasi-stationary population of particles is responsible for a "quiescent" flux level, while flares result from a uniform injection and/or acceleration of relativistic electrons over a time interval Δt. The evolution of the particle distribution is governed by the radiative cooling through synchrotron emission which dominates in the X-ray band. As the radiative losses are energy dependent, that is, the radiative lifetime of electrons is inversely proportional to the emitted frequency, low-energy photons are expected to lag high-energy photons (e.g., Urry et al. 1997; Takahashi et al. 1996). In particular, within this simple scenario, it is possible to relate the observed time lag to the physical parameters of the source (see also Tavecchio, Maraschi & Ghisellini 1998). In the observer's frame, this can be expressed as

$$B\delta^{1/3} = 223.5\left(\frac{1+z}{E_l}\right)^{1/3}\left[\frac{1-(E_l/E_h)^{1/2}}{\tau_{\rm obs}}\right]^{2/3} \text{G}$$

where E_l and E_h refer to the low and high X-ray energies (in units of keV), and $\tau_{\rm obs}$ (s) is the observed lag between E_l and E_h photons. Under the synchrotron cooling assumption, the observed time lag $\tau_{\rm obs}$ depends only on the magnetic field intensity B and the bulk Doppler factor δ of the radiating region. If we take E_l as 0.8 keV, E_h as 7 keV, and $\tau_{\rm obs} = 4.0$, 0.8, and 0.4 hr for each of the observations, our results would imply $B\delta^{1/3} \sim 0.32$, 0.94, and 1.49 G for SAX96,

ASCA94, and SAX97, respectively. Interestingly, Chiappetti et al. (1999) found that the model parameters derived through the fitting of the broadband spectrum during the SAX97 observation are consistent with those estimated from the observed soft lag.

A further piece of information is given by the trend between observed soft time lags and fluxes (see Fig. 10). If we, for example, assume that δ has not changed, the simplest scenario would suggest that B varied by a factor ~ 5 from SAX96 to SAX97. Although qualitatively consistent with the variation in the flux, this cannot quantitatively reproduce the observed correlation. In fact, under the (simplistic) assumptions of variations occurring only in the magnetic field, one would expect $F \sim B^{1+\alpha_x}$ and $B\delta^{1/3} \sim \tau_{\rm obs}^{-2/3}$, thus implying that the relation between intensity and lag is given by $F \sim \tau_{\rm obs}^{-2(1+\alpha x)/3}$ (assuming δ constant), where $\alpha_{\rm X}$ is the X-ray spectral index. For $\alpha_{\rm X} \sim 1.0$, we have $F \sim \tau_{\rm obs}^{-4/3}$. For example, the change in the lag by a factor ~ 10 from SAX97 to SAX96 would imply a flux variation of a factor ~ 22. However, the corresponding observed flux just changed by a factor ~ 1.4 in the 0.1–1.5 and 3.5–10 keV bands. The predicted relation between the lags and the fluxes under this hypothesis is also shown in Figures 10*a* and 10*c*, where it can be clearly seen that this is much flatter than that of the observed one between all of the observations. Therefore, as one might expect, other physical quantities, such as the density and energy spectra of the electron population and/or the Doppler factor, have to vary if the observed relation between flux and lag holds within the homogeneous synchrotron self-Compton scenario.

One more interesting piece of information for PKS 2155−304 is given by the good correlation found between variability parameters and source intensity. These have been plotted in Figure 11 as the fractional variability parameter ($F_{\rm var}$) and "doubling time" (T_2) against the source flux in the 1.5–10 keV band: as the source gets brighter, the average amplitude of variability is larger and the fastest variability timescale shorter. Although this is only a suggestive trend—given the limited statistics—it seems to indicate that the properties characterizing variability are not random. Any mechanism(s) invoked to account for (variable) radiative dissipation has to intrinsically produce this behavior. More observations with high time resolution clearly are required to confirm and quantify this trend.

We also (qualitatively) stress that the flux–time lag relationship could be associated with the importance of light-crossing effects with respect to the cooling timescales. A more intense flux could be associated with relatively efficient dissipation, such as, e.g., that occurring at a shock front, which—for a quasi-planar geometry (shock-in-jet model, in which a thin shock wave moves down a cylindrically symmetric jet; Marscher & Gear 1985)—could imply that light-crossing effects do not dominate and, thus, there would be small time lags. A low source state, more similar to the quiescent underlying jet emission, might be associated with an acceleration/injection of particles in a larger region: because of significant light-crossing effects, the observed variability would be smoother and result in larger time lags between different frequencies.

Finally, let us consider the information given by the PDS, which statistically characterizes the variability of a source. It should be noted that with the available data it is not easy to determine through the PDS the typical (or minimum) variability timescale as the light curves on small time bins become very noisy. More powerful techniques, e.g., the structure function, have to be considered. In general, the amplitude of variability decreases as the timescales become shorter. Previous studies, mainly of Seyfert galaxies, show that their PDS can be approximated by power laws with slopes ranging between 1.5 and 2.0 (e.g., McHardy 1999), thus providing valuable constraints by which to discriminate among possible models. However, the PDS of BL Lac objects has not yet been well studied in the X-ray band. The best determined PDS has been derived by Tagliaferri et al. (1991) for PKS 2155−304 using *EXOSAT* observations. An average power-law slope of $\alpha \sim 2.5$ was obtained for the PDS in the 1–6 keV band, which, however, reduced to 1.9 after the removal of the linear trend (as required in that case). Our analysis shows, over the same temporal frequencies, that the slope of the average PDS from each observation is consistent within 1 σ with that of the "detrended" PDS derived from *EXOSAT* data. The fastest variability timescale inferred from the PDS may reach ~ 1000 s, although this is largely uncertain because of the noisy PDS. We note that this timescale is consistent with that estimated from the PDS of the *EXOSAT* observations (Tagliaferri et al. 1991). Moreover, Paltani (1999) recently determined a similar minimum timescale (~ 600 s) from the

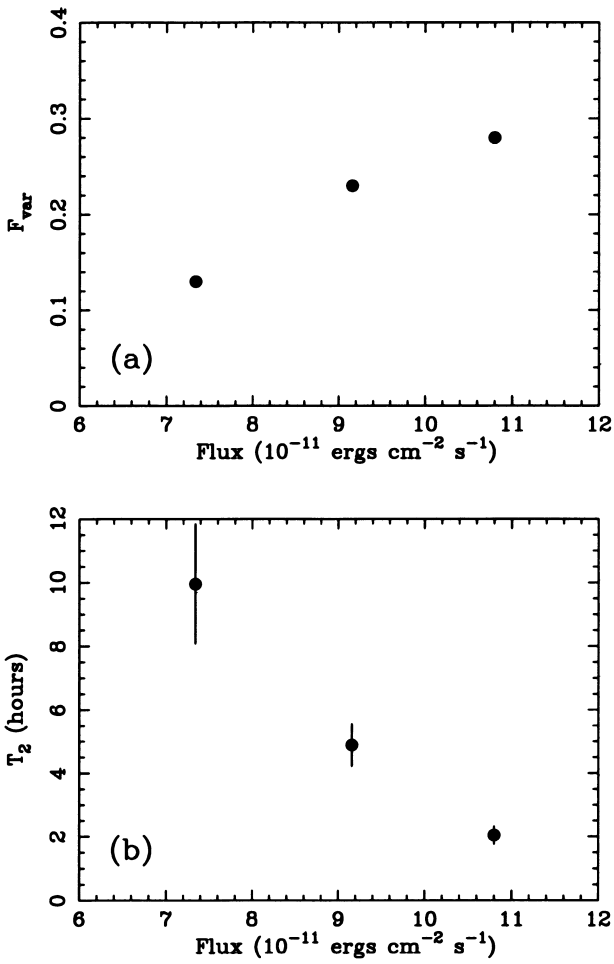

FIG. 11.—(*a*) Correlation between $F_{\rm var}$ and flux in the 1.5–10 keV band. The value of $F_{\rm var}$ during the flare of the ASCA94 is reported (see the text for details); (*b*) behavior of the "doubling time" (T_2) vs. the flux in the 1.5–10 keV band.

EXOSAT data by using the structure function. Interestingly, the most rapid variability estimated from the "doubling time" in the three observations occurred on a similar timescale ($\sim$1 hr), at least in SAX97. Of course, longer and uninterrupted X-ray monitoring will be crucial for constraining the PDS of blazars.

7. CONCLUSIONS

We have considered three long-duration X-ray light curves of PKS 2155−304 with high time resolution and have performed a detailed time-series analysis on them. The intensities in soft and medium X-rays are always well correlated, but with significantly different soft lags, suggesting that variability properties are time dependent and/or different mechanisms responsible for the variability may be at work. The three light curves presented here, which are sampled over short timescales, do not seem to show any direct correspondence with the overall/long-term variability properties of the source, as suggested by the two closely similar *ROSAT* light curves with about 5 yr separation discussed by Brinkmann & Siebert (1999).

The most important conclusions presented in this paper can be summarized as follows.

1. PKS 2155−304 shows several well-defined symmetric X-ray flares with similar rising and declining timescales. The amplitude of variability increases with increasing frequency. Very rapid variability events are not found on timescales of less than 1 hr.

2. The average PDS of SAX97 has significantly more power than those relative to the other two observations, indicating that PKS 2155−304 was more variable in this period. In addition, the rapid timescales and average amplitudes of variability may correlate with the source intensity, in the sense that higher brightnesses correspond to shorter timescales and larger amplitudes.

3. The interband X-rays are highly correlated in all cases but show different soft time lags, which may possibly be correlated with the source intensity. During SAX96, the source was in a relatively low state and showed the longest soft lag ($\sim$4 hr) recorded so far at X-ray wavelengths in BL Lac objects. The SAX97 light curves, which correspond to a high state, do not show significant time lag, while the ASCA94 light curves present intermediate time lag.

4. Within the simple homogeneous synchrotron (self-Compton) model for PKS 2155−304, the time lags could be interpreted as related to the cooling timescale of the relativistic emitting electrons, although the simplest change in the field intensity cannot quantitatively account for the observed dependence of lag on intensity.

5. The variability of the (X-ray) interband soft time lags of PKS 2155−304 is reminiscent of variations of lags between the UV and X-ray bands observed during the 1991 and 1994 multiwavelength campaigns (Edelson et al. 1995; Urry et al. 1997).

We thank the anonymous referee for constructive comments. Y. H. Z. and A. C. acknowledge the Italian MURST for financial support. This work was done partly in the research network "Accretion onto black holes, compact stars, and protostars" funded by the European Commission under contract number ERBFMRX-CT98-0195.

REFERENCES

Boella, G., Butler, R. C., Perola, G. C., Piro, L., Scarsi, L., & Bleeker, J. A. M. 1997a, A&AS, 122, 299
Boella, G., et al. 1997b, A&AS, 122, 327
Brinkmann, W., & Siebert, J. 1999, in ASP Conf. Ser. 159, BL Lac Phenomenon, ed. L. O. Takalo (San Francisco: ASP), 168
Chadwick, P.M., et al. 1999, ApJ, 513, 161
Chiaberge, M., & Ghisellini, G. 1999, MNRAS, 306, 551
Chiappetti, L., et al. 1999, ApJ, 521, 552
Edelson, R. A. 1992, ApJ, 401, 516
Edelson, R. A., et al. 1995, ApJ, 438, 120
Edelson, R. A., & Krolik, J. H. 1988, ApJ, 333, 646
Edelson, R., & Nandra, K. 1999, ApJ, 514, 682
Frontera, F., Costa, E., Dal Fiume, D., Feroci, M., Nicastro, L., Orlandini, M., Palazzi, E., & Zavattini, G. 1997, A&AS, 122, 357
Georganopoulos, M., & Marscher, A. P. 1998, ApJ, 506, L11
Giommi, P., et al. 1998, A&A, 333, L5
Hayashida, K., et al. 1998, ApJ, 500, 642
Hufnagel, B. R., & Bregman, J. N. 1992, ApJ, 386, 473
Makino, F., et al. 1996, in Röngtenstrahlung from the Universe, ed. H. U. Zimmermann, J. E. Trümper, & H. Yorke (MPE Report 263; Garching: MPE), 413
Manzo, G., Giarrusso, S., Santangelo, A., Ciralli, F., Fazio, G., Piraino, S., & Segreto, A. 1997, A&AS, 122, 341
Maoz, D., & Netzer, H. 1989, MNRAS, 236, 21
Marscher, A. P., & Gear, W. K. 1985, ApJ, 298, 114
Mastichiadis, A., & Kirk, J. M. 1997, A&A, 320, 19
McHardy, I. M. 1999, in ASP Conf. Ser. 159, BL Lac Phenomenon, ed. L. O. Takalo (San Francisco: ASP), 155
Padovani, P., & Giommi, P. 1995, ApJ, 444, 567
Paltani, S. 1999, in ASP Conf. Ser. 159, BL Lac Phenomenon, ed. L. O. Takalo (San Francisco: ASP), 293
Parmar, A. N., et al. 1997, A&AS, 122, 309
Pesce, J. E., et al. 1997, ApJ, 486, 770
Peterson, B. M., Wanders, I., Horne, K., Collier, S., Alexander, T., & Maoz, D. 1998, PASP, 110, 660
Pian, E., et al. 1997, ApJ, 486, 784
Press, W. 1978, Comments Astrophys., 7, 103
Press, W., et al. 1992, Numerical Recipes: The Art of Scientific Computing (2d ed.; Cambridge: Cambridge Univ. Press)
Rodríguez-Pascual, P. M., et al. 1997, ApJS, 110, 9
Sreekumar, P., & Vestrand, W. T. 1997, IAU Circ., 6774, 2
Tagliaferri, G., Bao, G., Israel, L., Stella, L., & Treves, A. 1996, ApJ, 465, 181
Tagliaferri, G., Stella, L., Maraschi, L., Treves, A., & Celotti, A. 1991, ApJ, 380, 78
Takahashi, T., et al. 1996, ApJ, 470, L89
Tanaka, Y., Inoue, H., & Holt, S. S. 1994, PASJ, 46, L37
Tavecchio, F., Maraschi, L., & Ghisellini, G. 1998, ApJ, 509, 608
Treves, A., et al. 1999, in ASP Conf. Ser. 159, BL Lac Phenomenon, ed. L. O. Takalo (San Francisco: ASP), 184
Urry, C. M., et al. 1997, ApJ, 486, 799
Vestrand, W. T., Stacy, J. G., & Sreekumar, P. 1995, ApJ, 454, L93